

# Fine structure collision strengths and line ratios for [Ne v] in infrared and optical sources

Michael Dance<sup>\*</sup>, Ethan Palay<sup>†</sup>, Sultana N. Nahar, Anil K. Pradhan

*Department of Astronomy, The Ohio State University, Columbus, OH 43210, USA*

Accepted xxxxxx Received xxxxxx; in original form xxxxxx

## ABSTRACT

Improved collision strengths for the mid-infrared and optical transitions in Ne v are presented. Breit-Pauli R-Matrix calculations for electron impact excitation are carried out with fully resolved near-threshold resonances at very low energies. In particular, the fine structure lines at 14  $\mu\text{m}$  and 24  $\mu\text{m}$  due to transitions among the ground state levels  $1s^2 2s^2 2p^3 \ ^3P_{0,1,2}$ , and the optical/near-UV lines at 2973, 3346 and 3426  $\text{\AA}$  transitions among the  $^3P_{0,1,2}, \ ^1D_2, \ ^1S_0$  levels are described. Maxwellian averaged collision strengths are tabulated for all forbidden transitions within the ground configuration. Significant differences are found in the low temperature range  $T_e < 10000$  K for both the FIR and the optical transitions compared to previous results. An analysis of the 14/24  $\mu\text{m}$  ratio in low-energy-density (LED) plasma conditions reveals considerable variation; the effective rate coefficient may be dominated by the very low-energy behaviour rather than the Maxwellian averaged collision strengths. Computed values suggest a possible solution to the anomalous mid-IR ratios found to be lower than theoretical limits observed from planetary nebulae and Seyfert galaxies. While such LED conditions may be present in infrared sources, they might be inconsistent with photoionization equilibrium models.

**Key words:** Gaseous Nebulae – Optical Spectra: H II Regions – Line Ratios: Atomic Processes – Atomic Data

## 1 INTRODUCTION

Several ionization stages of carbon-like ions provide useful diagnostics in the mid- to far-infrared (MIR-FIR) spaceborne observations, as well as prominently observed optical lines from ground based instruments. Nebular plasmas are generally the most common sources of these lines arising from forbidden transitions within the levels of the ground configuration of C-like ions (viz. Dopita and Sutherland 2003, Pradhan and Nahar 2011). Owing to much lower extinction than O/UV lines, the MIR and FIR reveal spatially extended sources to much greater depths. Therefore, in recent years space based observatories have provided added impetus to the analysis of MIR and FIR lines observed by *Spitzer*, *Herschel* and *Sofia*. In addition to molecular clouds photoionized by hot stars into nebulae, a much wider variety of astronomical objects whose physical conditions may be explored with mid-IR [Ne v] lines. These range from active galactic nuclei (Melendez *et al.* 2011, Perez-Beaupuits *et al.* 2011, Stern *et al.* 2012, Smith *et al.* 2012), metal-rich H II

regions (Furness *et al.* 2010), dusty environments of Ultra-Luminous-Infrared-Galaxies (ULIRGs, Houck *et al.* 2004, 2005; Nagao *et al.* 2011), and blue compact dwarf galaxies (Izotov *et al.* 2012).

H II regions in general, and planetary nebulae (PNe) in particular, are the testing ground as well as points of application of forbidden line ratios diagnostics with respect to temperature, density, and chemical abundances. The PNe are relatively bright and apparently simple objects that act as astrophysical laboratories to study basic atomic processes. However, several previous studies have discussed problems regarding [Ne v] lines (Clegg *et al.* 1987, Oliva *et al.* 1996, van Hoof *et al.* 2000). Based on the MIR 14/24  $\mu\text{m}$  line ratio, Rubin *et al.* (2001) and Rubin (2004) pointed out that for a number of PNe the observed values lie much lower than theoretically possible emissivity ratios at standard nebular temperatures and densities. More recently, in studies of spectral energy distributions in active galactic nuclei (AGN) using high-ionization mid-IR lines, a number of observations also reveal anomalous 14/24  $\mu\text{m}$  line ratios found to be below the theoretical limit (viz. Melendez *et al.* 2011, Tommasin *et al.* 2010, Weaver *et al.* 2010, Pereira-Santaella *et al.* 2010). Although the line forming regions in Seyfert galaxies may be dust obscured, the lower than predicted ratios are not

<sup>\*</sup> Present Address: Biomedical Program, University of Toledo, Toledo, Ohio, USA.

<sup>†</sup> Corresponding author

countenanced by derived mid-IR extinction (Li and Draine 2001). It is important to address this issue in order to use observed [Ne v] line ratio as density diagnostics, as the emissivity ratios indicate. Moreover, a deviation from theoretical limits of the otherwise clean and uncluttered spectral [Ne v] lines also renders the determination of mid-IR extinction uncertain (Melendez *et al.* 2011).

The analysis of the MIR and FIR space observations still rests on our understanding of nebular astrophysics. Forbidden lines are the primary diagnostics for low-temperature and low-density plasmas. In principle, the atomic physics is relatively straightforward: electron impact excitation of low-lying levels followed by radiative decay via magnetic dipole or electric-quadrupole transitions. These are the only two parameters required for simple collisional-radiative models, usually involving no more than the few levels of the ground configuration. However, it is well known that the electron impact excitation collision strengths and the relevant transition probabilities need to be calculated to high accuracy in order to determine the temperature-density regimes in the source. For example, C-like ground configuration  $1s^2 2s^2 2p^3$  gives rise to 3 LS terms and 5 fine structure levels  $^3P_{0,1,2}, ^1D_2, ^1S_0$ . In an earlier study, Palay *et al.* (2012) showed that near-threshold resonances in the collision strengths of C-like  $\phi 3$  make significant contribution to fine structure transitions. Rather elaborate computations including relativistic and resonance effects are necessary in order to delineate resonances and obtain accurate rate coefficients. In this work, we study the transitions in the Ne v ion and find similar effects. As Rubin *et al.* (2001) and Rubin (2004) have noted, different sets of collision strength data available in literature (viz. Lennon and Burke 1991, 1994; Griffin and Badnell 2000) did not resolve the discrepancy in the 14/24 ratio lying below the theoretical low density limit. The aim of this paper is to re-examine the Ne v collision strengths and line ratios computed using the Breit-Pauli-R-Matrix (BPRM) method (Berrington *et al.* 1995), with particular emphasis on the MIR lines under low-energy-density (LED) conditions. In order to examine the theoretical behaviour, we also extend the calculations to  $T_e < 1000\text{K}$ , not considered in previous works. Based on the more accurate data computed herein, the results should enable revised interpretation of MIR [Ne v] lines and originating plasma environments.

## 2 THEORY AND COMPUTATIONS

A brief theoretical description of the BPRM calculations is as follows (a discussion of the general methodology and application to atomic processes is given, for example, in Pradhan and Nahar 2011).

### 2.1 The Breit-Pauli approximation

The relativistic BPRM Hamiltonian is given as

$$H_{N+1}^{\text{BP}} = \sum_{i=1}^{N+1} \left\{ -\nabla_i^2 - \frac{2Z}{r_i} + \sum_{j>i}^{N+1} \frac{2}{r_{ij}} \right\} + H_{N+1}^{\text{mass}} + H_{N+1}^{\text{Dar}} + H_{N+1}^{\text{so}} \quad (1)$$

where the last three terms are relativistic corrections, respectively:

**Table 1.** Levels and energies ( $E_t$ ) of target (core ion) Ne V

	Level	$J_t$	$E_t$ (Ry) NIST	$E_t$ (Ry) SS
1	$1s^2 2s^2 2p^2 (^3P)$	0	0.0	0.
2	$1s^2 2s^2 2p^2 (^3P)$	1	0.003758	0.0030391
3	$1s^2 2s^2 2p^2 (^3P)$	2	0.010116	0.011366
4	$1s^2 2s^2 2p^2 (^1D)$	2	0.276036	0.30391
5	$1s^2 2s^2 2p^2 (^1S)$	2	0.582424	0.57413
6	$1s^2 2s 2p^3 (^5S^o)$	2	0.8052	0.71604
7	$1s^2 2s 2p^3 (^3D^o)$	3	1.60232	1.62957
8	$1s^2 2s 2p^3 (^3D^o)$	2	1.60296	1.62932
9	$1s^2 2s 2p^3 (^3D^o)$	1	1.60316	1.62929
10	$1s^2 2s 2p^3 (^3P^o)$	2	1.89687	1.92363
11	$1s^2 2s 2p^3 (^3P^o)$	1	1.89687	1.92340
12	$1s^2 2s 2p^3 (^3P^o)$	0	1.89719	1.92328
13	$1s^2 2s 2p^3 (^1D^o)$	2	2.46556	2.59326
14	$1s^2 2s 2p^3 (^3S^o)$	1	2.54576	2.64956
15	$1s^2 2s 2p^3 (^1P^o)$	1	2.76854	2.88988
16	$1s^2 2s 2p^4 (^3P)$	2	3.76063	3.86076
17	$1s^2 2s 2p^4 (^3P)$	1	3.76778	3.86807
18	$1s^2 2s 2p^4 (^3P)$	0	3.77085	3.87155
19	$1s^2 2s 2p^4 (^1D)$	2		4.13816
20	$1s^2 2s 2p^4 (^1S)$	0		4.74472

$$\begin{aligned} \text{the mass correction term, } H^{\text{mass}} &= -\frac{\alpha^2}{4} \sum_i p_i^4, \\ \text{the Darwin term, } H^{\text{Dar}} &= \frac{Z\alpha^2}{4} \sum_i \nabla^2 \left( \frac{1}{r_i} \right), \\ \text{the spin-orbit interaction term, } H^{\text{so}} &= Z\alpha^2 \sum_i \frac{1}{r_i^3} \mathbf{l}_i \cdot \mathbf{s}_i. \end{aligned} \quad (2)$$

Eq. (2) represents the one-body terms of the Breit interaction. In addition, another version of BPRM codes including the two-body terms of the Breit-interaction (Pradhan and Nahar 2011; W. Eissner and G. X. Chen, in preparation) has been developed, and is employed in the present work.

### 2.2 Ne V target representation

The coupled channel method embodied in the BPRM approximation is crucially dependent on the accuracy of the wavefunctions of the N-electron target ion included to represent the (N+1)-electron (e + ion) system. We employ the general purpose atomic structure code SUPERSTRUCTURE (Eissner *et al.* 1974) to compute a wavefunction expansion including the first 20 fine structure levels. Table 1 compares the calculated eigenenergies with experimental values tabulated by the U.S. National Institute of Standards and Technology ([www.nist.gov](http://www.nist.gov)).

The spectroscopic levels and configurations included in the (e + Ne v) wavefunction expansion are as in Table 1. The full configuration-interaction basis set optimized with SUPERSTRUCTURE is (Eissner *et al.* 1974, Nahar *et al.* 2003):  $[1s^2] 2s^2 2p^2, 2s 2p^3, 2s^2 2p 3s, 2p^4, 2s^2 2p 3p, 2s^2 2p 3d, 2s^2 2p 4s, 2s^2 2p 4p, 2s 2p^2 3s, 2s 2p^2 3p, 2s 2p^2 3d, 2s^2 3s^2, 2s^2 3p^2, 2s^2 3d^2, 2s^2 4s^2, 2s^2 4p^2, 2s^2 3s 3p, 2s^2 3s 4s, 2s^2 3p 3d, 2p^3 3s, 2p^3 3p, 2p^3 3d$ . Although the computed energies are generally within a few percent of the observed values, the latter are used in the BPRM calculations to ensure precise resonance positions relative to the Ne v target thresholds. The collision strengths were computed employing the extended BPRM codes including a full representation of the two-body Breit terms (Eissner and

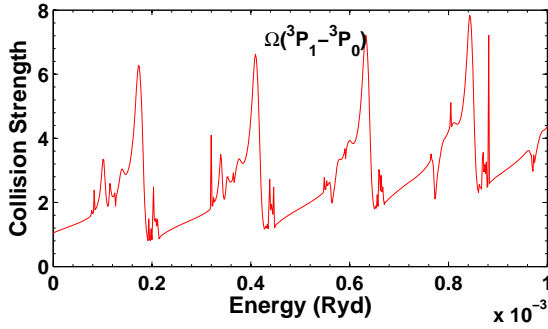


**Figure 1.** Rydberg series of near-threshold resonances in the collision strength for the fine structure transition  $2p^2(^3P_0 - ^3P_1)$  corresponding to the  $24 \mu\text{m}$  FIR line. A fine mesh order  $10^{-6}$  Ryd was used to fully resolve the  $(^3P_2, ^1D_2, ^1S_0)nl$  resonances, necessary for accurate rate coefficients at low temperatures.

Chen 2012). It is important to ensure convergence of collision strengths with respect to partial waves and energy resolution. Total (e + ion) symmetries up to  $(LS)J\pi$  with  $J \leq 19.5$  were included in the calculations, though it was found that the collision strengths for all forbidden transition transitions converged for  $J \leq 9.5$ . A very fine energy mesh of  $\Delta E < 10^{-6}$  Rydbergs was used to resolve the near-threshold resonances.

### 2.3 Effective collision strengths

The effective collision strengths or rate coefficients are computed by convolving the collision strengths over a Maxwellian function at a given electron temperature  $T_e$  as

$$\Upsilon_{ij}(T_e) = \int_0^\infty \Omega_{ij}(\epsilon) \exp(-\epsilon/kT_e) d(\epsilon/kT_e), \quad (3)$$

where  $E_{ij}$  is the energy difference and  $\Omega_{ij}$  is the collision strength for the transition  $i \rightarrow j$ . Later we discuss LED plasma conditions where the effective collision strength may differ from the form in Eq. (3). The excitation rate coefficient is related to the effective collision strength as

$$q_{ij}(T_e) = \frac{8.63 \times 10^{-6}}{g_i T_e^{1/2}} e^{-E_{ij}/kT_e} \Upsilon_{ij}(T_e), \quad (4)$$

where  $g_i$  is the statistical weight of the initial level.

## 3 RESULTS AND DISCUSSION

Collision strengths and line ratios are presented in this section. A discussion of possible implications for LED plasmas in general, and PNe in particular, is also given.

### 3.1 Ground state fine structure collision strengths

One of the main aims of the present calculations was complete resolution of resonance structures in near-threshold collision strengths. Fig. 1 shows the resolved Rydberg series of resonances in  $\Omega(^3P_0 - ^3P_1)$  converging on to the higher  $^3P_2, ^1D_2, ^1S_0$  levels. The calculations were carried out at an energy interval of  $10^{-6}$  Ryd. These resonances dominate the low-energy-temperature behaviour of the detailed, as well as

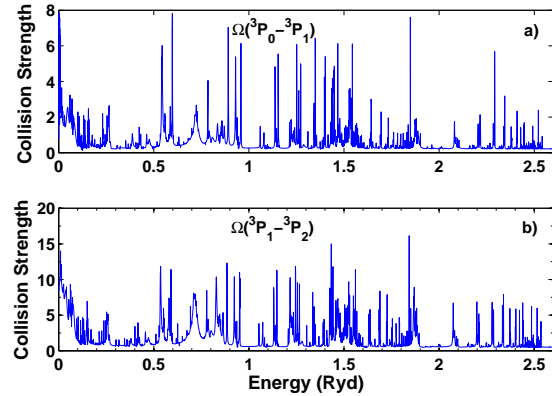


**Figure 2.** Collision strengths over extended energy ranges for fine structure transitions  $2p^2(^3P_0 - ^3P_1, ^3P_1 - ^3P_2)$  at a)  $24 \mu\text{m}$  b)  $14 \mu\text{m}$  respectively.

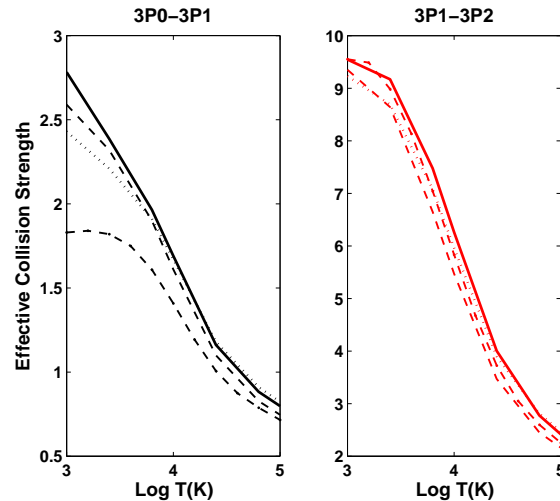


**Figure 3.** Maxwellian averaged effective collision strengths  $\Upsilon(T_e)$  for the transitions  $2p^2(^3P_0 - ^3P_1, ^3P_1 - ^3P_2)$  at a)  $24 \mu\text{m}$  b)  $14 \mu\text{m}$  (cf. Fig. 2): solid line. Dotted lines show previous results without relativistic effects (Lennon and Burke 1994); dash-dot and dashed lines show 20-level BPRM and 138-level ICFT results respectively (Griffin and Badnell 2000), available in the temperature range  $T_e > 1000$  K. The enhancements in present calculations are due to the fully resolved resonance structures near the threshold (cf. Fig. 1).

the averaged, collision strengths. The corresponding  $24 \mu\text{m}$  line is the one most affected. Fig. 2 shows the results over an extended energy range for  $\Omega(^3P_0 - ^3P_1)$  and  $\Omega(^3P_1 - ^3P_2)$ . Particularly noteworthy is the significant rise close to thresholds for both transitions.

The Maxwellian averaged collision strengths are plotted in Fig. 3 (solid curve), and compared with previous results from Lennon and Burke (1994, dotted curve) and two sets of calculations by Griffin and Badnell (2000). The latter work employed two different approximations, a 20-level BPRM calculation (dash-dot curve) and a more extensive intermediate-coupling fine structure transformation (ICFT, dashed curve) that is essentially non-relativistic (as in Lennon and Burke 1994) but incorporates relativistic

terms perturbatively via an algebraic transformation. For the 24  $\mu\text{m}$  transition, we find differences of up to 30% at the lowest temperatures with the otherwise similar previous 20-level BPRM results, most likely attributable to improved resolution at very low energies in the present calculations. Differences no larger than 10% are found for the 14  $\mu\text{m}$  transition between all sets of calculations.

Present calculations are also carried out at  $T_e < 1000\text{K}$ , not considered in previous works. Since we have taken particular care to fully resolve the near-threshold collision strengths, the effective collision strengths should be limited only by the intrinsic accuracy of the BPRM calculations and not by numerical resolution of resonances. That is necessary in order to interpret the line ratio observations in cases where they do not fall in the nebular temperature range, as discussed next.

### 3.2 The 14/24 $\mu\text{m}$ emissivity ratio and observations

Owing to small differences in excitation energies, the fine structure line ratios due to transitions within the ground state levels  $^3P_{0,1,2}$  are not highly temperature sensitive in the typical nebular range around 10,000K. On the other hand, this emissivity ratio is highly density sensitive at typical nebular densities of  $10^{3-6} \text{ cm}^{-3}$ . Rubin (2004) has tabulated the 14/24 line flux ratio from a number of PNe, and noted that it falls *below* the theoretically possible value of approximately 1.0 in about half the observations. Fig. 4 shows the measured line ratios; the asterisks denote the derived densities for the PNe that fall very well on the 10,000 K emissivity ratio curve. However, the observed values from some of the anomalous PNe are seen as lying around the emissivity ratio curve at 1000K or lower, shown as vertical dashed band in Fig. 4. One can readily find low temperature curves vs. density that could account for these ratios lying below the 10,000K curve. Incidentally, variations by similar amounts in both transitions yield very good agreement with ratios at  $T_e > 10,000\text{K}$  with previous works (viz. Lennon and Burke 1994), shown in the right panel.

Based on this work we can rule out further uncertainties in the collision strengths. Fig. 4 illustrates the dichotomy between the PNe with normal density sensitivity of the 14/24 ratio, and a fair number of those that appear to correspond to much lower temperatures than that which characterizes typical nebular photoionization equilibrium. While the equilibrium models may not explain these values, it is worth examining the behaviour of line ratios in LED plasmas in general. Eq. (3) implies that

$$\lim_{T \rightarrow 0} \Upsilon(T) = \lim_{E \rightarrow 0} \Omega(E). \quad (5)$$

Between 1000-10,000K the Maxwellian factor involves exponential factor  $\exp(-E/kT_e)$  ranging from  $\exp(-158 E)$  to  $\exp(-15.8E)$  in Rydberg units. Therefore  $\Upsilon(T)$  depends entirely on the detailed behaviour of  $\Omega(E)$ . Furthermore, if we also consider that fact that low densities  $N_e \approx 10^2 \text{ cm}^{-3}$  may exist, a departure from the normal Maxwellian distribution under LED conditions is possible. Therefore, the rate coefficient would tend to follow the collision strengths *and* variations with resonance structures at very low energies close to excitation threshold(s). This suggestion is offered to re-examine non-equilibrium conditions that might prevail in

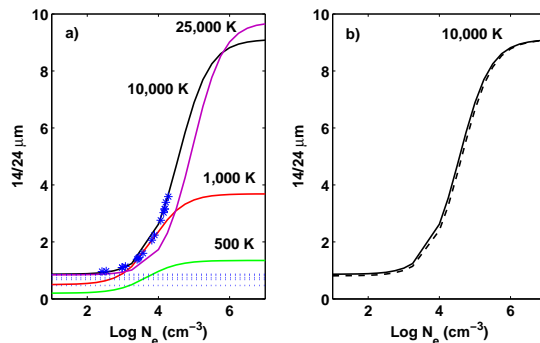


**Figure 4.** The density and temperature dependence of the 14/24  $\mu\text{m}$  line emissivity ratios: a) Solid lines represent line ratios at four temperatures. Asterisks denote observed line ratios from planetary nebulae (Rubin 2004), at  $T_e = 10,000 \text{ K}$  with assigned densities. Dotted lines represent observed line ratios that are out of range of typical nebular temperature-density range (Rubin 2004), except at much lower temperatures. b) solid curves are present results and the dashed lines are using the Lennon and Burke (1994) collision strengths. Large differences in line ratios are not found because of *systematic* differences of similar magnitude for both lines between previous and present rate coefficients.

LED plasma sources, which may also not have established a Maxwellian distribution. The emitted line intensity would then depend on the actual kinetic energy and number density of electrons at a given energy. In addition, the electron and ion temperatures may differ, i.e.  $T_e \neq T_i$ .

### 3.3 [Ne v] optical collision strengths and line ratios

Collision strengths for forbidden optical transitions within ground configuration levels are shown in Fig. 5:  $^3P_1 - ^1D_2$ ,  $^3P_2 - ^1D_2$ ,  $^1S_0 - ^1D_2$  at  $\lambda\lambda$  3345.8, 3425.9, 2972.8, respectively. Resonance structures due to Ne v target excitation thresholds given in Table 1 manifest themselves at all energies, and need to be considered in the calculation of averaged collision strengths. Whereas the agreement with previous works (Lennon and Burke 1994, Griffin and Badnell 2000) is found to be satisfactory, generally 10-15% or better, for some of the relatively weak transitions there are marked differences. Fig. 6 compares the present results for the Maxwellian averaged collision strengths for two transitions,  $^3P_0 - ^1D_2$  and  $^3P_0 - ^1S_0$  that do not directly correspond to observed lines but enter in the solution of rate equations for line emissivities. The differences are found to be rather large. Nevertheless, the important optical line ratios are not significantly affected, as shown in Fig. 7. The blended emissivity ratio  $(3426+3346)/2973$  differs little from those derived from earlier values from Lennon and Burke (1994).

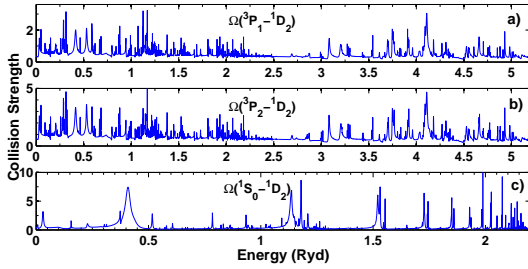
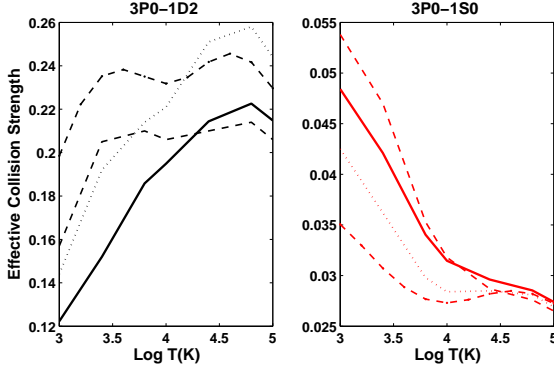
### 3.4 Maxwellian averaged collision strengths

In Table 1, we present the effective collision strengths (Eq. 3) for the 10 transitions among the ground configuration levels and their wavelengths. The tabulation is carried out at a range of temperatures typical of nebular environments,



**Table 2.** Effective Maxwellian averaged collision strengths

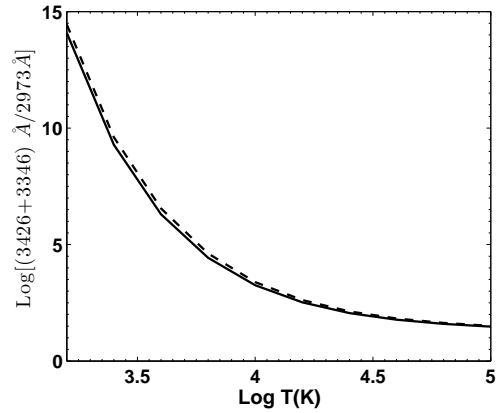
Transition	$\lambda$	$\Upsilon(100)$	$\Upsilon(500)$	$\Upsilon(1000)$	$\Upsilon(5000)$	$\Upsilon(10000)$	$\Upsilon(20000)$	$\Upsilon(30000)$
$^3P_0 - ^3P_1$	14 $\mu\text{m}$	2.72(0)	3.02(0)	2.78(0)	2.09(0)	1.69(0)	1.28(0)	1.07(0)
$^3P_2 - ^3P_0$	9 $\mu\text{m}$	2.70(0)	3.00(0)	3.16(0)	2.56(0)	1.93(0)	1.34(0)	1.04(0)
$^3P_2 - ^3P_1$	14 $\mu\text{m}$	8.48(0)	9.18(0)	9.55(0)	8.02(0)	6.26(0)	4.49(0)	3.60(0)
$^1D_2 - ^3P_0$	3301.3 $\text{\AA}$	1.23(-1)	1.20(-1)	1.22(-1)	1.80(-1)	1.95(-1)	2.09(-1)	2.19(-1)
$^1D_2 - ^3P_1$	3345.8 $\text{\AA}$	3.76(-1)	3.67(-1)	3.69(-1)	5.37(-1)	5.84(-1)	6.27(-1)	6.58(-1)
$^1D_2 - ^3P_2$	3425.9 $\text{\AA}$	6.61(-1)	6.46(-1)	6.47(-1)	9.22(-1)	9.97(-1)	1.07(0)	1.1(0)
$^1S_0 - ^3P_0$	-	4.60(-2)	4.82(-2)	4.84(-2)	3.58(-2)	3.15(-2)	2.98(-2)	2.94(-2)
$^1S_0 - ^3P_1$	1574.8 $\text{\AA}$	1.35(-1)	1.42(-1)	1.42(-1)	1.04(-1)	9.13(-2)	8.73(-2)	8.69(-2)
$^1S_0 - ^3P_2$	1592.3 $\text{\AA}$	2.24(-1)	2.35(-1)	2.35(-1)	1.73(-1)	1.53(-1)	1.47(-1)	1.45(-1)
$^1S_0 - ^1D_2$	2972.8 $\text{\AA}$	3.51(-1)	4.51(-1)	4.88(-1)	6.69(-1)	6.26(-1)	6.33(-1)	6.87(-1)


**Figure 5.** Collision strengths for the forbidden optical transitions  $2p^2(^3P_1 - ^1D_2, ^3P_2 - ^1D_2, ^1S_0 - ^1D_2)$  at 3346, 3426, 2973  $\text{\AA}$  respectively

**Figure 6.** Maxwellian averaged collision strengths  $\Upsilon(T_e)$  for the transitions  $2p^2(^3P_0 - ^1D_2, ^3P_0 - ^1S_0)$ : Solid lines. Dotted lines show previous results without relativistic effects (Lennon and Burke 1994); dashed and dash-dot lines show 20-level BPRM and 138-level ICFT results respectively (Griffin and Badnell 2000)

including the low temperature range  $T \leq 1000\text{K}$  not heretofore considered.

### 3.5 Conclusion

New calculations for [Ne v] collision strengths are reported including relativistic and resonance effects at very low energies that affect the low temperature rate coefficients not heretofore calculated. In particular, a precise delineation of near-threshold resonance structures has a significant effect on the mid-IR 14/24  $\mu\text{m}$  line emissivities. However, low-density theoretical limits of the ratios computed at typical nebular temperatures  $T_e \approx 10,000\text{K}$  are still higher than


**Figure 7.** Blended [Ne v] optical line ratio (3346+3426)/2973 vs.  $T_e$  at  $N_e = 10^3 \text{ cm}^{-3}$ . Despite significant differences in the collision strengths the optical emissivity ratios agree with those using earlier data by Lennon and Burke (1994) owing to systematic enhancements in the same direction.

the anomalously low values of observations from a number of PNe discussed by Rubin *et al.* (2001) and Rubin (2004). Since the Maxwellian averaged collision strengths generally decrease with temperature, and simulate the behaviour of collision strengths at low energies, it is suggested that non-equilibrium conditions corresponding to LED plasma conditions might possibly account for the low observed 14/24 ratios. In any case, the low temperature rate coefficients for  $T_e < 10,000\text{K}$  are likely to be uncertain owing to resonances at low energies.

The [Ne v] forbidden optical collision strengths are generally in good agreement with previous works, and the prominent line ratios are not much influenced. Finally, as noted in the previous work on  $\phi 3$  lines (Palay *et al.* 2012), for higher temperatures  $T > 20,000\text{K}$  proton impact excitation of the ground state fine structure levels  $^3P_{0,1,2}$  needs to be taken into account; at lower temperatures the excitation rate coefficient due to electrons far exceeds that due to protons (Ryans *et al.* 1999).

Collision strengths for all 190 transitions among energy levels in Table 1 may be obtained from Ethan Palay (palay.5@buckeyemail.osu.edu).

**ACKNOWLEDGMENTS**

The computational work was carried out at the Ohio Supercomputer Center in Columbus Ohio. This work was partially supported by a grant from the NASA Astrophysical Research and Analysis program. EP would like to gratefully acknowledge a Summer Undergraduate Research Program grant from the Ohio State University.

**REFERENCES**

- Berrington K. A., Eissner W. & Norrington P. H., 1995, *Comput. Phys. Commun.* 92, 290
- Clegg R.E.S., Harrington J.P., Barlow M.J., Walsh J.R., 1987, *Astrophys. J.* , 314, 551
- Dopita M. A. & Sutherland R. S., 2003, *Astrophysics of the Diffuse Universe*, Springer-Verlag
- Eissner W. & Seaton M. J., 1972, *J. Phys. B* 5, 2187
- Furness J. P. *et al.* , 2010, *Mon. Not. R. astr. Soc.* , 403, 1433
- Griffin D. and Badnell N. R., 2000, *J. Phys. B* , 33, 4389
- Houck J. R. *et al.* , 2004, *Astrophys. J. Suppl. Ser.* , 154, 18
- Houck J. R. *et al.* , 2005, *Astrophys. J. Lett.* , 622, L105
- Izotov Y.I., Thuan T.X. and Privon G., 2012, *Mon. Not. R. astr. Soc.* , 427, 1299
- Lennon D. J. and Burke V.M., 1991, *Mon. Not. R. astr. Soc.* , 251, 628
- Lennon D. J. and Burke V. M., 1994, *Astron. Astrophys. Suppl. Ser.* , 103, 273
- Li A, & Draine B.T., 2001, *Astrophys. J.* , 554, 778
- Liu X., Shapley A. E., Coil A. L., Brenchmann J. and Ma C.-P., 2008, *Astrophys. J.* , 678, 758
- Melendez M., Kraemer S.B., Weaver K.A., and Mushotzky R.F, 2011, *Astrophys. J.* , 738, 6
- Nahar S.N., Eissner W., Chen G.-X., Pradhan A. K., 2003, *Astron. Astrophys.* , 487, 789
- Nahar S. N., Pradhan A. K., Montenegro M., Eissner W., 2011, *Phys. Rev. A* , 83, 053417
- Nagao T., Maiolino R., Marconi A., and Matsuhara H., 2011, *Astron. Astrophys.* , 526, A149
- Oliva E., Paquali, A., Reconditi M., 1996, *Astron. Astrophys.* , 305, L21
- Perez-Beaupuits J.P., Spoon H.W.W., and Smith J.D., 2011, *Astron. Astrophys.* , 536, 56
- Periera-Santaella M., Diamond-Stanic A.M., Alonso-Henrro A., & Rieke G.H. 2010, *Astrophys. J.* , 725, 2270
- Pradhan A. K. and Nahar S. N., 2011, *Atomic Astrophysics and Spectroscopy*, Cambridge University Press
- Rubin R.H., *et al.* , 2001, ASP Conference Series, 247, 479
- Rubin R.H., 2004, ASP Conference Proceedings of IAU Symposium No. 217, 190
- Ryans R. S. I., Foster-Woods V. J., Reid R. H. G., Keenan F. P., 1999, *Astron. Astrophys.* , 345, 663
- Smith K.L., Shields G.A., Stevens A.C., and Rosario D.J., 2012, *Astrophys. J.* , 752, 63
- Stern D. *et al.* , 2012, *Astrophys. J.* , 753, 30
- van Hoof P.A.M., Beintema D.A., Verner D.A. and Ferland G.J., 2000, *Astron. Astrophys.* , 354, L41
- Weaver K.A., *et al.* 2010, *Astrophys. J.* , 716, 1151